SSC23-S3-11

The Rogue alpha and beta mission: operations, infrared remote sensing, LEO data processing, and lessons learned from three years on orbit with two laser communication-equipped 3U CubeSats

Authors: Dee W. Pack, Pradeep Thiyanaratnam, Brian S. Hardy, Tom Freeze, John R. Santiago, David Pietrowski, Michael Leon
The Aerospace Corporation
2310 E. El Segundo Blvd., El Segundo, CA 90245; (310) 336-5645
dee.w.pack@aero.org

ABSTRACT

The Aerospace Corporation's Rogue-alpha, beta program was a rapid prototyping demonstration aimed at building and deploying an infrared remote sensing capability into low Earth orbit within 18 months. The two satellites and their data were then used for three years as an experimental testbed for future proliferated low Earth orbit (pLEO) constellations. Their launch took place on November 2, 2019, followed by boost and deployment of two identical spacecraft (Rogue-alpha and beta) by the Cygnus ISS cargo vessel into circular 460-km, 52° inclined orbits on January 31, 2020. The primary sensors were 1.4-micron band, InGaAs short wavelength infrared (SWIR) cameras with 640x512 pixels and a 28° field-of-view. The IR sensors were accompanied by 10-megapixel visible context cameras with a 37° field-of-view. Star sensors were also tested as nighttime imaging sensors. Three years of spacecraft and sensor operations were achieved, allowing a variety of experiments to be conducted. The first year focused on alignment and checkout of the laser communication systems, sensor calibration, and priority IR remote sensing objectives, including the study of Earth backgrounds, observation of natural gas flares, and detection of rocket launches. The second year of operations added study of environmental remote sensing targets, including severe storms, wildfires, and volcanic eruptions, while continuing to gather Earth backgrounds and rocket launch observations. The final year emphasized advanced data processing and exploitation techniques applied to collected data, using machine learning and artificial intelligence for tasks such as target tracking, frame co-registration, and stereo data exploitation. Mission operations continued in the final year, with an emphasis on collecting additional rocket launch data, and higher frame rate backgrounds data. This report summarizes the Rogue alpha, beta mission's outcomes and presents processed IR data, including the detection and tracking of rocket launches with dynamic Earth backgrounds, embedded moving targets in background scenes, and the use of pointing-based registration to create fire line videos of severe wildfires and 3D scenes of pyrocumulonimbus clouds. Lessons learned from the experimental ConOps, data exploitation, and database curation are also summarized for application to future pLEO constellation missions.

INTRODUCTION

The Rogue-alpha,beta program built and launched two 3-Unit CubeSats into low earth orbit (LEO) to perform experimental remote sensing observations, calibration studies, and spacecraft operations investigations. The two spacecraft are referred to as Rogue-α and Rogue-β and a designation of AeroCube15-A and AeroCube15-B is also used at times for the spacecraft, including in online orbital element databases. An initial paper detailed the engineering effort that successfully designed, built, tested, and launched the two CubeSats in 18 months, fulfilling the programmatic goal of a rapid prototype demonstration.[1] A second paper summarized our first year of orbital operations, including on-orbit, satellite-to-satellite alignment of our lasercom system, stellar radiometric calibration techniques, some characterization of our primary sensor's 1.4μm short-wavelength infrared (SWIR), water overtone band, Earth backgrounds collection, and other remote sensing observations.[2] Notable highlights from the first year of operations included the first CubeSat infrared observations of rocket launches with unique observations of Falcon 9 and Soyuz flights above the Earth horizon.[2] A third paper emphasized environmental observation results from our second year of operations and presented video imaging results from hurricanes, tropical cyclones, tornadic thunderstorms and extreme wildfires, including pyrocumulonimbus cloud observations.[3] In our final year of operations we added significantly to our observations of rocket launches and Earth backgrounds, and have focused on analysis of our unique, high frame rate Earth imaging data. The additional space launches observed included Soyuz, Long March, Atlas V and Falcon 9 events, bringing the total rockets observed in flight to eight. We obtained our first daytime launch observations, including tracking launches in cloudy scenes and across the Earth limb.

Operations continued until the failure of Rogue-β's on-board flash memory storage card on November 30, 2022, and the reentry of Rogue-α on February 7, 2023 (Rogue-β reentered on February 10, 2023). In what follows, we briefly describe the Rogue CubeSats and payloads, the mission timeline events and experiments, map and describe significant remote sensing observations and a complete list of rocket launch observations. Emphasis is placed on newly collected data, and data subjected to new analysis during the last year of operations.

Spacecraft Overview

The Rogue-α,β satellites were identical 3-Unit (3U) CubeSats with dimensions of 34 x 11 x 11 centimeters and mass of approximately 3.7 kg. The avionics, sensors, 200Mbps lasercom, and 500Kbps UHF RF communications payloads, were evolved from those used in prior AeroCube projects with reuse of as many parts and systems as possible to enable the rapid prototype construction.[4-6] The remote sensing payloads consisted of a SWIR InGaAs camera and a small visible imaging context camera, both located on the nadir face. A narrow field of view star camera was oriented at 90° relative to the remote sensing payloads. This ensured a good space-pointed view could be achieved for accurate star fixes when the primary payload was pointed at the Earth horizon along the direction of orbit (fore or aft). For other pointing ConOps, such as pointing at a ground target during an orbital pass, careful planning usually allowed good NFOV star observations to be obtained during all or most of an orbital pass. Two additional star sensors were packaged on the zenith face pointed at 45° off the zenith and oriented at 90° from each other. These additional compact zenith star sensors were carried over from prior AeroCube missions. They added redundancy and provided star fixes in the approximately 5% of collections when the NFOV sensor could not be placed in a favorable orientation relative to the Sun or sunlit Earth. Figure 1 illustrates the spacecraft design and highlights how the compact sensors, avionics, and the compact laser communications payload were packaged.

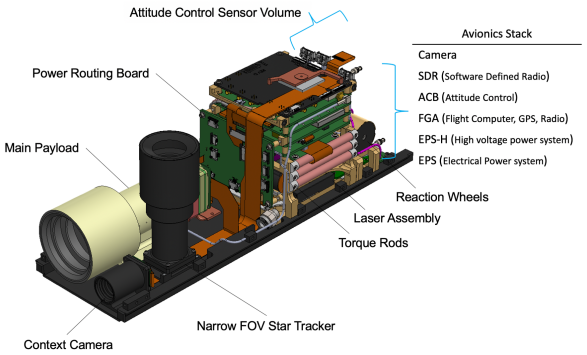

Figure 1. The Rogue-α,β spacecraft architecture

The photo in Figure 2 shows the two completed 3U spacecraft in the laboratory. The solar wings are deployed in this image. Body solar panels and one of the three patch antennae are visible. The spacecraft are equipped with 3 patch antennae, 2 for UHF radios (one of which is for a higher bandwidth software defined radio), and one for GPS reception. The primary SWIR sensor is prominent on the nadir face in Figure 2, accompanied by a smaller visible context camera. A great deal of capability was packed into a small spacecraft volume for this project, which allowed the affordable launch of two identical sensor platforms.[1,2]

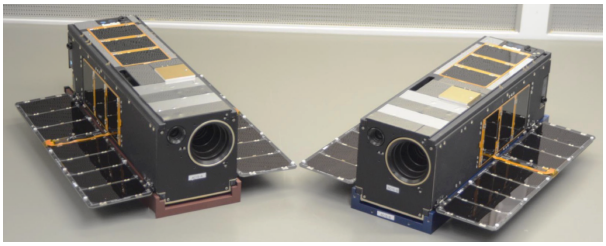

Figure 2. The completed Rogue-α,β spacecraft

Payload Overview

The Rogue-α,β remote sensing payload consisted of a short wavelength infrared imager comprised of an Aerospace Corporation custom-designed, athermal refractive optical telescope and sunshade, integrated with a commercially available SWIR camera core and an off-the-shelf 1.4μm spectral filter. A separate visible 10-megapixel context camera was included, with a comparable, but somewhat larger field of view compared to the infrared camera. The SWIR primary payload was a FLIR Tau SWIR 640x512 pixel, thermoelectrically cooled, InGaAs camera core. An earlier version of this camera was flown with success as an unfiltered, space-based night vision camera as part of the Cubesat Multispectral Observing System (CUMULOS), an earlier project.[4,5] A custom, five-lens, athermal refractive telescope was designed to insure low-distortion infrared imaging, and to allow proper placement of a spectral filter between the lens and the camera focal plane assembly. A custom sunshade was fitted to the optical assembly and can be seen flush with the nadir face in Figures 1 and 2. This had a solar keep out angle of approximately 40 degrees for stray light reduction.

A narrow bandpass 50nm wide Edmonds Optics spectral filter was selected with transmission near the 1.4μm atmospheric water absorption band. This filter was measured at 1.398-1.452μm (50% transmission points) and is somewhat like the cirrus bands on weather and environmental monitoring satellites. The VIIRS M9 cirrus band, centered on the water overtone band at 1.38μm, has a narrower, 15nm wide bandpass, and is designed to see only high clouds and to detect subtle

cirrus ice cloud features. Our Rogue SWIR band retained some ability to see to the ground, especially under favorable zenith angle geometries, and high or dry atmospheric conditions. MODTRAN Mid-Latitude Summer modeled sea level transmissions, at zero and 50° zenith angles, were: 0.0471 and 0.0211. For Mid-Latitude Winter the same transmissions were: 0.2014 and 0.1297. Because of atmospheric water absorption, the 1.4μm band provided some discrimination ability between low, medium, and high, optically thick clouds at a given look angle from the reflected solar signal. This made the band useful for studying cloud scenes and structure from low Earth orbit (LEO), while retaining the ability to detect bright infrared sources such as rocket launches, as well methane flares and wildfires at low altitudes under favorable viewing conditions.

The visible context camera consisted of a monochromatic ON Semiconductor 12-bit Si:CMOS 10-megapixel on-chip focal plane array with no filter. It was fitted with a commercial 12mm focal length lens and a small custom sunshade assembly designed to provide a similar solar keep out angle to the SWIR primary sensor. The context camera complemented the infrared camera by providing panchromatic visible images to aid in interpreting cloud and Earth scenes acquired in the 1.4μm SWIR band especially in humid conditions.[2] In addition to observing daytime scenes, the visible camera's exposure time could be increased for nighttime imaging.[3]

A few experiments were conducted using the NFOV star camera as a low-light sensor for nighttime remote sensing.[3] This sensor used a SiOnyx extended red "black silicon" focal plane with a nominal sensitivity of 0.4-1.2 μm. This focal plane also allowed the sensor's use for on-orbit lasercom alignment.[2]

The camera control electronics which ran the primary sensors as well as the star sensors could control up to 5 sensors simultaneously. GPS time stamps were applied to individual frames from the camera payloads and were accurate to approximately ± 10ms.

Table 1 lists important sensor payload parameters. The sensor payloads were characterized by compact fast optics and modestly wide fields of view (approximately 28° diagonally for the 1.4μm camera). The NFOV star sensor has a finer angular resolution to enable subpixel pointing of the IR remote sensing payload. The whole assembly fit into less than 1.5 U of spacecraft volume.[2]

Mission Operations

Using pre-programed agile pointing (enabled by the 3-axis stabilized bus), ample on-board data storage (1GB of RAM storage and 8GB of onboard flash memory storage), and the 200Mbps lasercom downlink, the Rogue-alpha,beta CubeSats were able to record multiple experiments with multiple minutes of video and later transmit results during ground receive station passes. Experiments were programmed one at a time, and two to three experiments per week were conducted, limited by staffing and the need to manage on-board storage.

Table 1: Rogue-α,β Sensor Payload Parameters

Camera / Payload Parameter	SWIR	VIS	NFOV Star Sensor
Lens F#	2.77	2	2.5
Focal Length (mm)	25	12	50
Pixel Pitch (μm)	15	1.67	5.6
FPA dimensions (pixels, bits)	640x512, 14	3840x2748, 12	1280x720, 12
Altitude (km)	460	460	460
Nadir Pointed GSD (m)	276	256, 128, or 64*	52
Nadir Pointed Swath (km)	177x141	247x177	66x37
FOV (degrees)	21.7x17.5	30.1x21.8	8.2x4.6
IFOV (mrad)	0.60	0.56, 0.28, 0.14*	0.11
Filter (μm)	1.398-1.452	none	None

*VIS camera pixels are coadded 4x4 in our standard operations mode with higher resolution options available when desired.

Prior work summarized our exploration of different modes of tasking our fast-framing LEO sensors.[2,3] These modes included: 1) fore, aft, port and starboard horizon-pointed, multi-minute image collections that maximized area coverage, 2) using the two spacecraft in formation, when closely spaced in orbit, pointed fore and aft to conduct stereo observations of cloud structure and altitude, 3) point-and-stare imaging for several minutes aimed at bright natural gas flares, environmental events (predicted storm locations, wildfires, and active volcanic regions), and publicly announced space launches. IR frame rates used during imaging experiments were varied from 1hz, 3hz, 4hz and 20hz to study frame stabilization and backgrounds suppression. Visible sensor data were collected to provide context imagery at a rate of 1 visible frame per 10, 20 or 40 SWIR frames. These data proved quite helpful in understanding Earth and cloud backgrounds, as well as weather, smoke, and terrain features.

Just prior or following remote sensing experiments the Rogue-α,β spacecraft were slewed to point at dark space to collect dark frames, typically at the North Galactic pole. This was necessary for dark offset correction due to the lack of a shutter on the SWIR camera. Observation of IR stars for radiometric calibration were taken in several experimental observations. Metric calibration also used stars and was refined with ground features.[2,3,7]

Mission Planning Cycle

The Rogue-α,β mission's remote sensing planning cycle used the Aerospace Corporation's *Satellite Orbital Analysis Program* (SOAP) and related software libraries in conjunction with a dynamic list of remote sensing target objectives. Experiment goals determined daytime or nighttime conditions, tasking mode, desired satellite look angles, duration of observation, frame rates and whether one or two satellites were tasked. For space launch observations, web scraping of scheduled takeoff times and locations was employed, supplementing manual tracking of publicly announced space launches in the news media. Rocket launch schedules required close monitoring since delays caused launches to both slip out of, and into, our two satellites orbital coverage.

For the first year of operations, we followed a prioritized mission plan of data collection for calibration, static IR source observations, diverse Earth backgrounds, stereo observations, rocket launches, and wildfire and severe weather data collection. Following a successful first year with all primary mission goals achieved, our extended operations period focused on pursuing more rocket observations, particularly daytime ones below the horizon, taking longer background data collections, collecting data at higher frame rates, and observing as many severe storms, wildfires, and other interesting IR observations as possible. We also performed nighttime sensor observations with the context camera and star sensors.

Data Pipeline and Archive

Development of a data processing pipeline and data archive was an important part of the Rogue-α,β project. We pursued an approach that created multiple formats at a cost of multiplying the data volume stored. The raw imaging data were downlinked via lasercom, parsed, and binary images of raw level zero (L0) data were created in FITS and TIFF formats. These raw L0 and their corresponding dark frames were processed to corrected counts (L1 data). The FITS format was primarily used in the stellar calibration work which used astronomical software requiring FITS files.[7]

Metadata were stored as JSON companion files. Information in these included GPS timestamps, sensor settings and sensor pointing information, derived from star sensor data sampled every 4.4 seconds and rate gryo data. Pointing metadata were downlinked via RF and recombined on the ground with the imagery data.

L2 georegistered data were produced by combining pointing metadata quaternions with the imaging data to create HDF5 files with ECEF line-of-sight pointing vectors for every pixel. These data products were used for pointing and tracking studies and three-dimensional processing. GEOTIFFS and ground footprint vector files were also created. The L2 metadata also included other information derived from the sensor pointing knowledge and on-board GPS location and timing data, such as satellite position in latitude, longitude and altitude, satellite zenith angle, solar zenith angle and solar scattering angles at the edges and center of the focal plane field-of-view. Radiometric calibration factors were applied, when needed, using our stellar observation results.[2,7] The processed data archive is approximately 2.1 TB in size.

The products that have seen the most use have been HDF5 files, TIFFS and GEOTIFFS. We wrote our HDF5 files and associated metadata following a standard DoD remote sensing format which allowed existing processing tools to be readily used. Video files were also created for displaying and reviewing multi-frame data. Optimal display of the 12-bit visible camera data, and 14-bit SWIR data, was usually possible via linear histogram stretching. Logarithmic or dynamic stretching algorithms are employed when both dim and bright scene features needed to be displayed. More sophisticated tools were developed for displaying and performing tracking and three-dimensional processing.

The next section maps and summarizes the Rogue-α,β flight experiment campaign. We then summarize our rocket launch observations, novel aircraft observations, and environmental observations, with an emphasis on newer data and the data processing techniques being applied to the fast-framing low-earth orbit IR data.

ROGUE-α,β REMOTE SENSING EXPERIMENTS

Map Summary of Rogue-α,β Ground Footprints

Figures 3A and 3B show an updated map of the ground imaging footprints for most of our Earth-pointed SWIR data collections from Rogue-α (A) and Rogue-β (B). Most of these collects varied from 2 to 15 minutes in duration. The footprints are indicative of the collection modes utilized. The fore or aft horizon-pointed, wide-field-of-view experiments present as strips of data, the length determined by their duration. Port or starboard horizon-pointed mode collections present as wider wedge-shaped polygons. Point-and-stare experiments often show a "butterfly" pattern ground footprint centered on their targets (storm centers, flares, fires, volcanic activity, or rocket launches). Clear examples of these include the California wildfire imaging experiments and the La Palma volcanic activity observations in the Canary Islands.[3] These observations start and end with a wide area view of the targeted region to the Earth horizon with the middle of the overpass

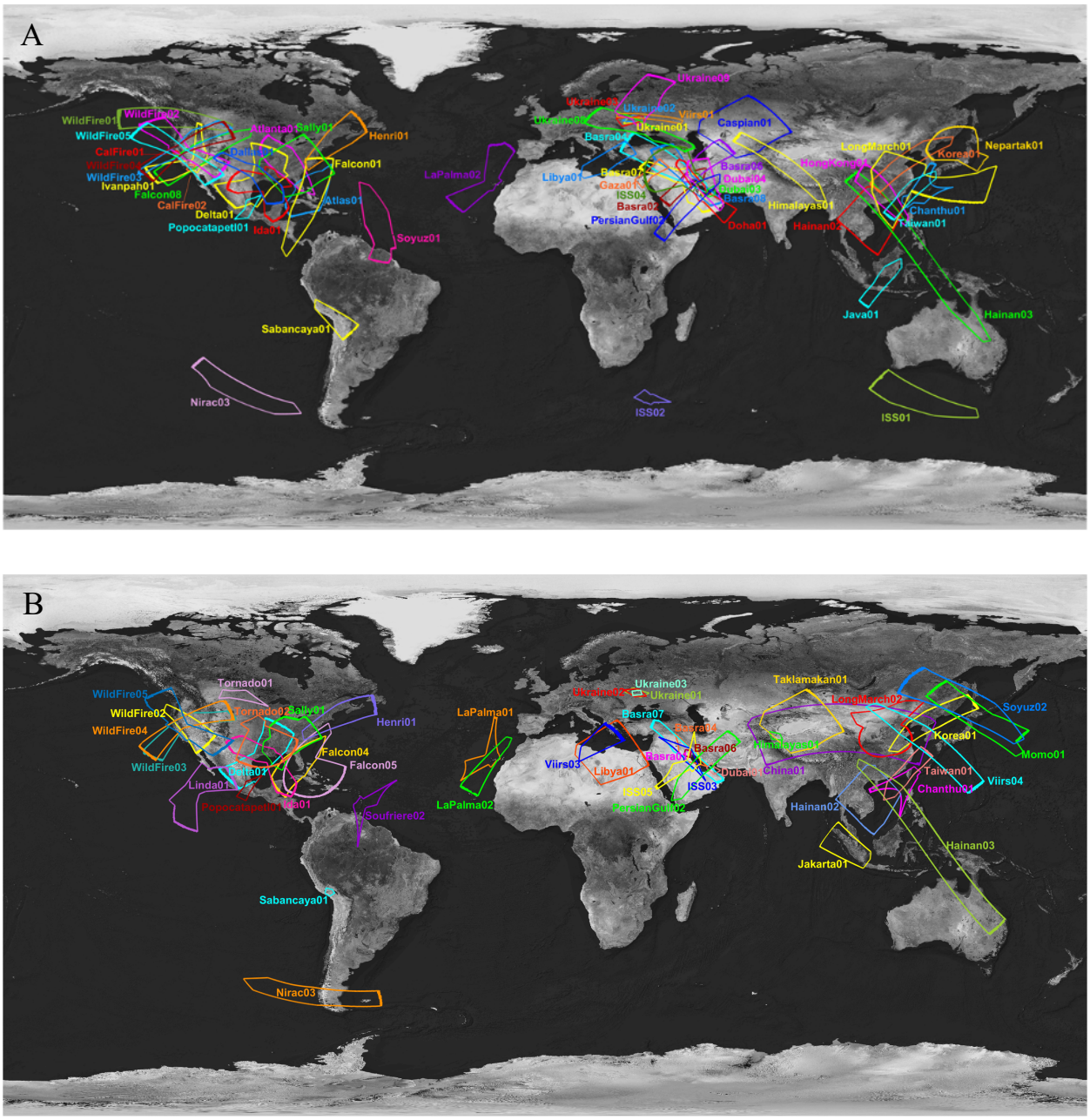

Figure 3: Remote Sensing Experiment Footprints from June 2020 – January 2023. A) Rogue-α. B) Rogue-β

covering a smaller region near nadir. Stereo and multi-satellite sequential observations observed in common by both Rogue alpha and beta satellites appear in both Figure 3 A and B footprint images. Highlights of these experiments from 2020 and 2021 were described in two prior papers.[2,3]

Data taken during conjunctions with other orbiting sensors were collected in both horizon pointed and point-and-stare mode. These account for some of the oddly placed, open ocean data collects, for which observing clouds at the exact same time was the goal. The concurrently taken, somewhat larger, visible sensor footprints, as well as the handful of star sensor nighttime imaging experiments, are omitted from the summary in Figure 3. Also not captured in the ground footprint map are the space-pointed collects used for dark frame collection, stellar calibration, lunar observations, and the above-the-horizon imaging portion of our space launch observation experiments.

Rocket Launch Observations

This section describes the Rogue-α,β space launch observations, the majority of which have not been documented previously. Publicly announced space launches were our experimental opportunities. The spacecraft were programmed to point their SWIR sensors to a latitude, longitude, altitude location at a specified time. These experiments were all carried out using point-and-stare mode, some with slight modifications to try to keep rockets within our field of view longer. collection started right before a scheduled launch or right before the sensor field of view to the target rose over the horizon. Sensor pointing would be maintained during orbit until recording stopped, or until the spacecraft was programmed to repoint to a new position down the expected trajectory. In some cases, two different IR sensor exposure times were programmed to ensure detection of a target of unknown intensity. This required a pause in data collection during which the contents of the 1GB of volatile memory were written to the 8GB flash storage drive. For most experiments, a single exposure time was selected. This varied if the observation was taken during daytime or nighttime, or if the expected position of the rocket target was above or below the Earth limb. Table 2 summarizes the eight space launches observed during the 2020-2022 Rogue-a,β mission operational period. Each of these rocket launch experiments presented different geometries, solar conditions, and orbital considerations. For some, liftoff occurred before the post-launch viewing opportunity, for others, one of the two CubeSats had excellent orbital geometry to observe the launch site at T0 (liftoff). No stereo opportunities presented during the mission (due to launch delays in some cases). Publicly released post-launch information, including launch videos, provided useful timing and telemetry information.

Table 2: Rocket Launch Experiments

Collect Name Satellite	UTC Launch Date:Time	Launch Vehicle Mission	Launch Location	Total Frames @ Frame Rate, Exposure Time	Stages Observed	Target View	Daytime or Nighttime
Falcon01 Rogue-α	10/18/2020: 12:25:57	Falcon 9 Starlink	Cape Canaveral, FL	361 @ 1hz, 20ms	2nd stage, 1st deorbit burn	ATH	Daytime
Soyuz01 Rogue-α	12/29/2020: 16:42:07	Soyuz ST-A Arianespace Flight VS25	Kourou, French Guiana	218 @ 1hz, 50ms	Core stage, (post boosters) + 2nd stage	ATH	Daytime
LongMarch01 Rogue-α	06/17/2021: 01:22:27	Long March 2F Shenzhou-12	Jiuquan, China	800 @ 1hz, 100ms	Only 2nd stage	ATH	Daytime
Soyuz02 Rogue-β	10/14/2021: 09:40:10	Soyuz-2.1b Arianespace OneWeb	Vostochny, Russia	321 @1 hz, 50ms	Boosters + 1st stage	BTH ATH	Nighttime
Falcon04 Rogue-β	01/31/2022: 23:11:14	Falcon 9 COSMO-SkyMed 2nd Gen. FM2	Cape Canaveral, FL	301 @ 1hz, 10ms	1st stage	BTH	Nighttime
Falcon05 Rogue-β	06/08/2022: 21:04	Falcon 9 Nilesat 301	Cape Canaveral, FL	361 @ 1hz, 5ms	1st stage (BTH), 2nd stage (ATH)	BTH ATH	Daytime
Falcon08 Rogue-α	08/12/2022: 21:40:20	Falcon 9 Starlink	Vandenberg SFB, CA	961 @ 4hz, 3ms	1st stage	BTH, ATH	Daytime
Atlas01 Rogue-α	10/04/2022: 21:36:00	Atlas V ULA SES-20, 21	Cape Canaveral, FL	921 @ 3hz, 2ms	Core RD180 + solid boosters	BTH	Daytime

Depending on timing, ascending, or descending passes of the two satellites 52° inclination, 460km circular orbits intersected differently with the targeted rocket launch trajectories. The simplest case was when the space sensor had line of sight to the launch pad at the beginning of the launch window and the rocket took off on time. For cases when the overpass was after the launch time, the pointing could still be directed at the pad, or directed down range if necessary. The observed rockets summarized in Table 2 were all quite large, high thrust space launch vehicles. The Falcon 9, and Soyuz vehicles used kerosene / liquid oxygen fueled boosters, core and second stages. The Atlas V had large solid rocket boosters and a kerosene / liquid oxygen core stage. The H_2 / liquid oxygen upper stage was not detected in this study. The Long March 2F, human-rated, Chinese space launch vehicle differed in that it used UDMH / N_2O_4 fueled boosters, core, and 2nd stages.

Our basic experimental goal was to take as much data on a given launch as possible given our orbital geometry, subject to data storage constraints. Data collection commenced approximately 1 minute prior to launch, or prior to our obtaining line of sight, and continued for a pre-programmed multi-minute period. Exposure times are summarized in Table 2 and varied from 2-100ms. We varied the exposure time based on: 1) whether the rockets were observed against cold space, 2) whether they were under daytime or nighttime conditions, 3) whether the target was a bright low-altitude afterburning rocket or a dimmer, smaller thrust, exoatmospheric upper stage, and 4) how much of the bright Earth limb was in the sensor field of view. As with our observations of clouds, flares, and wildfires some experimentation was necessary to determine optimal sensor settings, but our choices were all successful in detecting rocket signals. All launches observed were reported to have been successful and to have performed nominally.

Image processing

Rocket combustion signals at night, or above the horizon against a space background, were often readily detected manually by subtracting sequential frames. This suppressed bad pixels that might have escaped correction and is referred to as *FrameDiff*. We also combined spatial and temporal algorithms, followed by use of RX anomaly detection, to highlight launch signals of interest and used these in sequence. A Laplacian spatial filter was applied to single frames. A temporal difference filter was then applied (between the current frame and an average of a small number of preceding frames). Then RX anomaly detection is performed. This algorithm combination is referred to in what follows as *Fusion*. Applying the fusion algorithm first and then frame differencing to reduce detection of noisy pixels is referred to as *Fusion-FrameDiff*.

Pointing-based registration (PBR) of sequential frames was carried out for launches observed during daytime below the horizon. This was followed by sequential frame differencing to subtract cloud backgrounds and highlight the bright rocket emissions. This approach is referred to as *PBR-FrameDiff* and achieved good results for daytime space launches. Other approaches can be tested using the Rogue-α,β data. Artificial signals can also be embedded in the data, and more advanced algorithms tested and refined. Next, we summarize our eight launch observations and present illustrative snapshots of the unprocessed and processed data, tracks of the bright rockets using a manually initiated tracking algorithm, and the orbital geometry of the experiments.

Oct. 18, 2020, Falcon 9 Starlink Launch

Our first launch observation was of a SpaceX Starlink launch which presented an opportunity with a trajectory heading northeast from Florida. Liftoff at 12:25:57 UTC took place prior to arrival of the observing satellite.[2] Our Rogue-α spacecraft did not have line of sight to the launch pad at T0 as it orbited north on an ascending pass. The spacecraft was south of central America when it initially achieved line of sight to the Falcon second stage, already underway. The Rogue-α orbit then "chased" the 2nd stage up the coast of the United States. Observation of both the second stage burn and the first stage initial deorbit burn was achieved via pre-programmed pointing to a position off the coast of Cape Hatteras, North Carolina.[2] A snapshot of the observation and processed tracks at 12:32:38.41 UTC is shown in Figure 4. The single Merlin engine 2nd stage was tracked from 12:29:29.41-12:34:22.41 UTC. The shorter, lower altitude, brighter, three-Merlin engine, 1st stage deorbit RAM burn was also tracked for 19 seconds from 12:32:19.41-12:32:38.41 UTC.

Dec. 29, 2020, Soyuz ST-A Launch

A Soyuz launch out of French Guiana was targeted by Rogue-α in our second successful launch observation experiment. As in our first launch observation, the spacecraft had no line-of-site to the launch pad at T0. In this case, however, the launch headed northwest, and the satellite was on a descending pass, so the rocket was nominally heading into the satellite field of view, not away from it. As the satellite orbited towards the South American coastline, the core stage of the Soyuz was detected above the Earth horizon after the booster's thrusting had ceased and they had been separated from the spacecraft. Beginning at 16:44:47.41 UTC, the core stage was tracked from near the horizon, and then tracking continued into the second stage burn. Recording stopped at 16:47:00.40 UTC to dump data to flash memory. A snapshot of the observation at the end of the first collection and the processed track at 16:47:01.40 UTC is shown in Figure 5. A bright flash at 16:46:54.40 UTC was a likely staging transient.[2] The only information used to task this experiment was the opening of the launch window, the rough direction of launch for the mission, and the published characteristics of the launch vehicle. The spacecraft was programed to initially point at the Kourou launch center and collect data at 50ms exposure time and then repoint and collect more data at 100ms exposure time. The initial observation was paused shortly after the expected core stage burnout while collected data were written to flash memory storage. The satellite then repointed further west and started sensor operations again at 100ms exposure. The longer exposure times were chosen due to the smaller thrust of the Soyuz upper stage relative to that of the Falcon 9. The results of this second period of Soyuz observation from 16:48:02.38 - 16:48:36.37 UTC are shown in Figure 6. The two tasked exposure times were performed to insure some properly exposed data were obtained. The repointing at longer exposure was

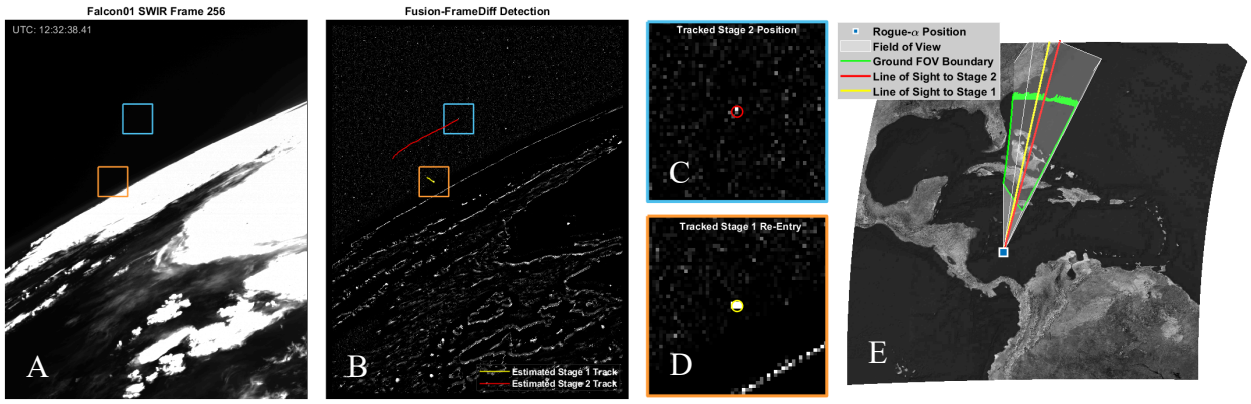

Figure 4. Oct 18, 2020, Falcon 9 Starlink launch at SWIR frame 256. A) Unprocessed, B) Processed tracks showing the second stage and the short 1st stage reentry burn. C) Processed detail of the 2nd stage and D) the bright 1st stage RAM burn tracks. E) Geometry of the observations.

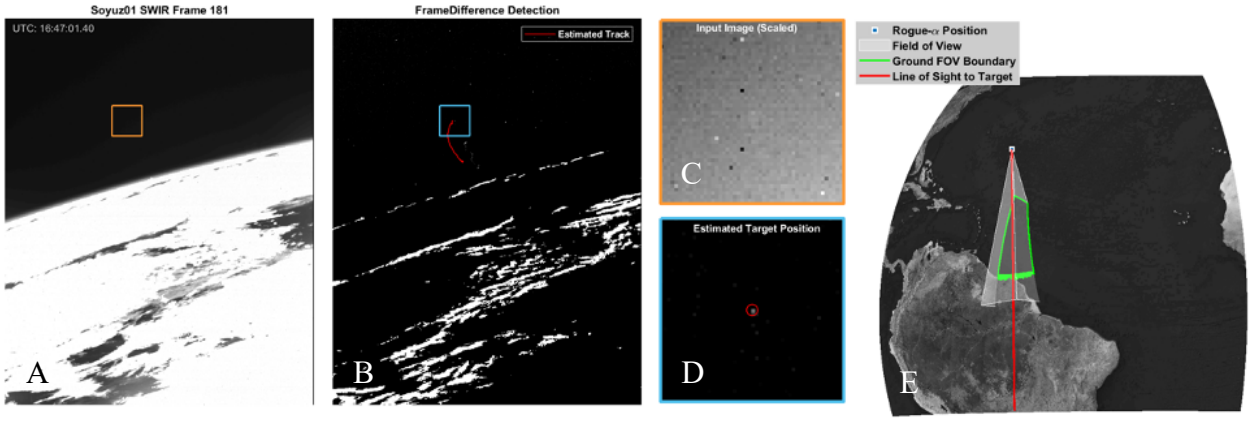

Figure 5. Dec 29, 2020, Soyuz ST-A Arianespace launch at SWIR frame 181. A) Unprocessed, B) Processed track showing the core stage dogleg maneuver ending with the beginning of the 2nd stage. C) Unprocessed and D) Processed detail. E) Geometry of the observation.

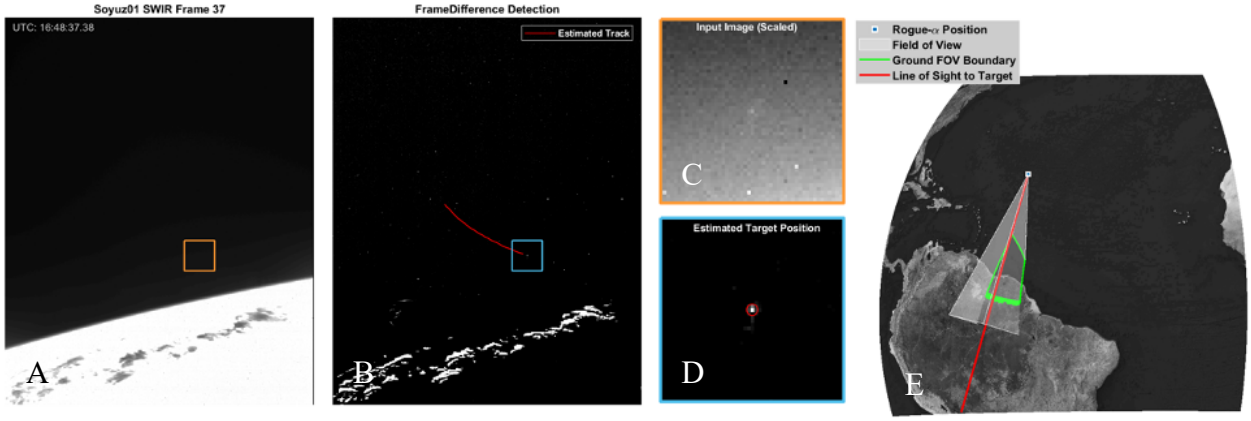

Figure 6. Dec 29, 2020, Soyuz ST-A Arianespace launch. Second longer exposure measurement at SWIR frame 37. A) Unprocessed, B) processed track showing the dimmer second stage. C) Unprocessed and D) Processed detail at end of track. E) Geometry of the second observation.

performed as a contingency to improve the line of sight to an unknown trajectory, and to observe the performance of a longer exposure time on a fast-moving orbital encounter. Both observations were successful. The 2020 Falcon 9 and Soyuz launches were described in more detail in our first launch operations paper.[2]

Jun. 17, 2021, Long March 2F Observation

The Long March 2F Shenzhou-12 mission was the first Chinese manned spaceflight to the new Tianhe core module of the Tiangong space station. The mission was widely covered in the media, as were past related launches. T0 was at 01:22:27 UTC, well before Rogue-α had line of sight to the pad on an ascending pass. The spacecraft was programed to point towards the launch site and data collection timed to start at 01:24:01.65 UTC and continue for 800 seconds This timing recorded data past the expected burnout of the upper stage, with coverage of the expected flight path. Snapshots of the data, track and geometry are shown in Figure 7. A "flash" in the dim signal at 01:30:05.60 UTC was likely related to the second stage engine cutoff and stage separation. The second stage was tracked from 01:29:14.60 - 01:30:12.60 UTC. Manual inspection found the dim signal slightly earlier, closer to the horizon.

Oct. 14, 2021, Soyuz 2.1b Launch

Rogue-β observed the nighttime launch of an Arianespace Soyuz OneWeb mission out of the Vostochny Cosmodrome, Russia. T0 was 09:40:10.356 UTC, 1 hour after local sunset and the rocket flew north after its ascent phase. This commercial launch was our first rocket observation opportunity for which we had line of sight directly to the launch pad at T0. Rogue-β pointed aft from over the Pacific Ocean southeast of Honshu, Japan and detected the bright Soyuz signal approximately 10 seconds after liftoff in Russia. The satellite was on a descending pass, flying away from the rocket, and tracked the launch from 09:40:20.47 - 09:43:53.47 UTC. A noticeable reduction in signal, but not loss of track, occurred at 09:42:12.47 UTC 127 seconds after launch, which lined up closely with the time noted in onboard camera video of the boosters being released.[8] Figure 8 shows the processed data and geometry at end of track. Since the core stage burn was not yet over, the track signal loss was likely due to the increasing range as the rocket flew north and Rogue-β orbited on a southeast heading.[9] The appearance of the nighttime scene was interesting, exhibiting a sunlit solar terminator region farther south of the launch site which receded out of the satellites field of view. A noticeable airglow layer emission in our 1.4μm band was also evident above the Earth limb and appears in the snapshot shown in Figure 8. Some ground static features from likely wildfires were also observed.

Jan. 31, 2022, Falcon 9 Cosmo-Skymed 2nd Gen. Launch

This Falcon 9 launch of a European radar satellite had a flight path heading southwest from Cape Canaveral. Rogue-β tracked the rocket from an ascending pass on a northeast heading, starting over South Carolina at 23:11:36.43 UTC and keeping track until 23:13:45:43, when the CubeSat subpoint was off the coast of Long Island, NY. The signal track dropped just after the main engine cutoff at T0 +2min 20 seconds.[10] The transition to the lower thrust Falcon 2nd stage, and the range-induced decreasing signal as the rocket headed in the opposite direction from the satellite, were the likely cause for the signal loss in our post-event tracking analysis. The observation occurred just after local sunset and was a stringent test of our tiny CubeSat sensor's solar rejection capability. Figure 9 shows the unprocessed data with bright sunlit clouds on the Earth limb, *Fusion* processed data, and the track geometry, mid-track at 23:12:49.43 UTC.

Jun. 8, 2022, Falcon 9 Nilesat 301 Launch

After two years of orbital operations, the timing of the Falcon 9 Nilesat 301 launch out of Cape Canaveral, Florida presented Rogue-β with our first opportunity to obtain a rocket observation during daytime below the horizon against a cloudy background. T0 was reported as 21:04 UTC and the rocket was first tracked emerging from clouds at 21:04:36.43 UTC as the CubeSat orbited over West Virginia heading northeast on an ascending pass traveling away from the launch site. From the SpaceX launch video telemetry, the rocket was at an altitude of approximately 2.5 km at time of detection.[10] After the initial ascent, the launch's azimuth headed east to place a communications satellite into a geosynchronous transfer orbit. After being tracked crossing bright, structured cloud backgrounds, the track ended at 21:06:15.42 UTC when the rocket signal was lost in saturated high cloud structure right before main engine cutoff. Video telemetry reported the rocket at an altitude of approximately 48.3km and speed of 6090km/hr at this time.[10] Figure 10 shows the data, track (using the pointing-based registration frame-difference technique) and the observation's geometry at a point in the middle of the track. The pictured single frame shows the rocket just before it passed over some cloud background structure across which it was successfully tracked. The dimmer Falcon 9 second stage was subsequently tracked above the horizon from 21:06:59.43 - 21:07:31.43 UTC. This second track ended when it flew out of the Rogue-β field of view which was still fixed at the launch site. The rocket was moving around 8000 km/hr at this point[10] and the CubeSat was over Maine.

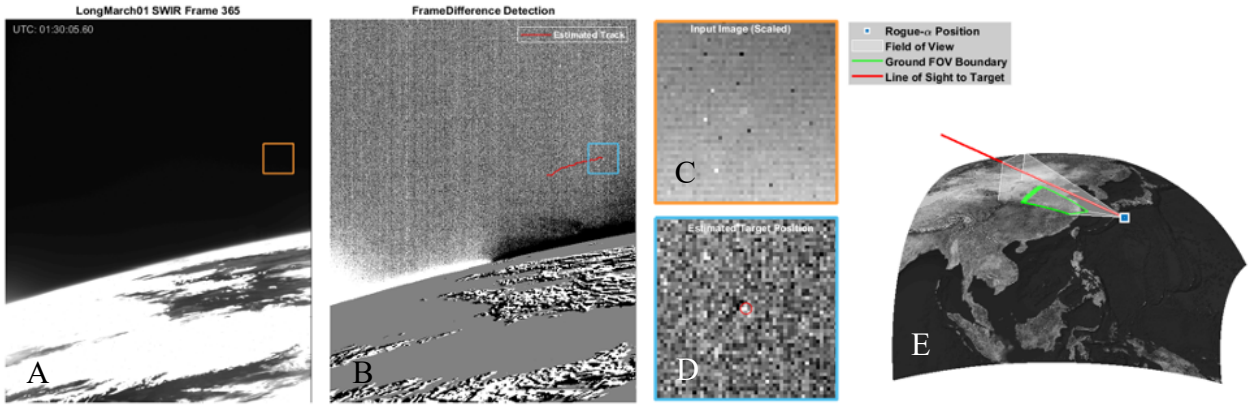

Figure 7. Jun 17, 2021, Long March 2F launch snapshot at frame 365 A) Unprocessed, B) Processed track showing the dimmer second stage. C) Unprocessed and D) Processed frame detail. E) Geometry of the observation.

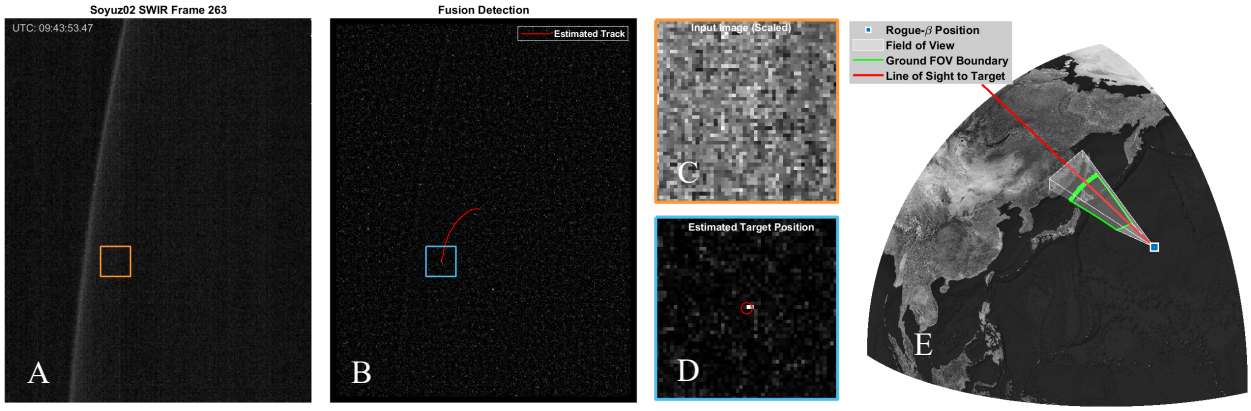

Figure 8. Oct 14, 2021, Soyuz 2.1b Arianespace launch at SWIR frame 263. A) Unprocessed, B) Processed track C) Unprocessed and D) Processed frame detail. E) Geometry of the observation.

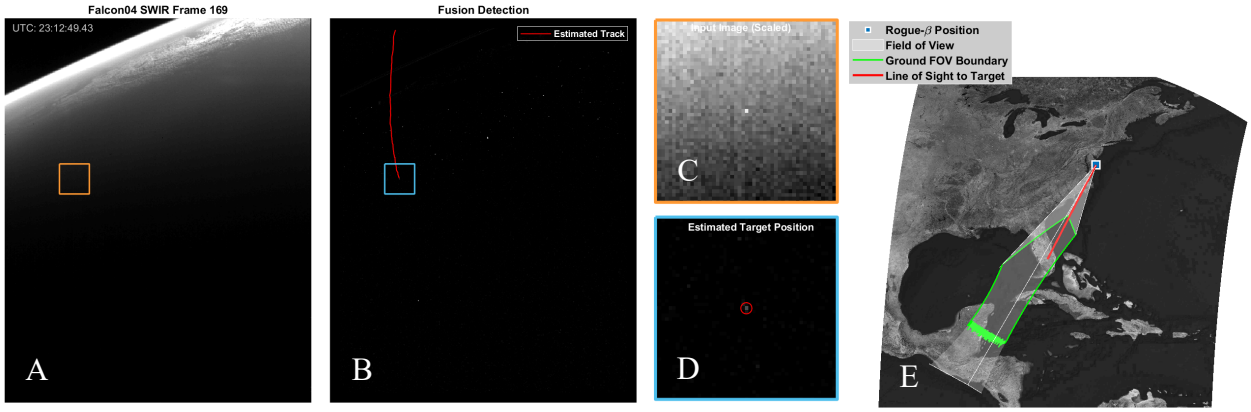

Figure 9. Jan 31, 2022, Falcon 9 COSMO-SKYMED FM2 2nd Generation launch snapshot at frame 169. A) Unprocessed, B) Processed track C) Unprocessed and D) Processed frame detail. E) Geometry of the observation.

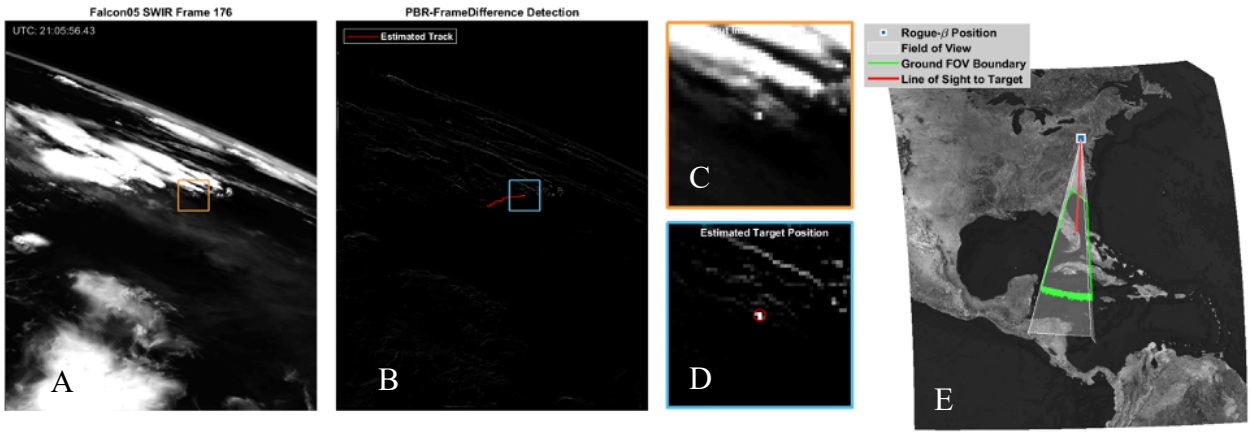

Figure 10. Jun 8, 2022, Falcon 9 Nilesat 301 Launch snapshot at SWIR frame 176. A) Unprocessed, B) Processed track C) Unprocessed and D) Processed frame detail. E) Geometry of the observation.

Aug. 12, 2022, Falcon 9 Starlink Launch

This daytime Falcon 9 Starlink mission out of Vandenburg Space Force Base launched at 21:40 UTC. Observation by Rogue-α was from a receding ascending pass pointed southwest towards the launch site. SWIR data were taken at 4hz. The launch was tracked from below the horizon starting at 21:40:55.19, through the Earth limb from 21:41:25.43 to 21:41:49.94, and slightly past the main engine cutoff to 21:42:40.44 UTC (MECO was reported by SpaceX at approximately 21:42:34)[11]. Weakening signal due to range, and the short 3ms integration time (selected for the daytime observation) likely accounted for loss of track. The CubeSat orbited from over Montana to Manitoba, Canada during the tracking interval, and had a long-range view of the rocket with a tail-on aspect angle. Figure 11 shows the data, track on the pointing-based registration frame difference processed data, and geometry at 21:42:32.94 UTC.

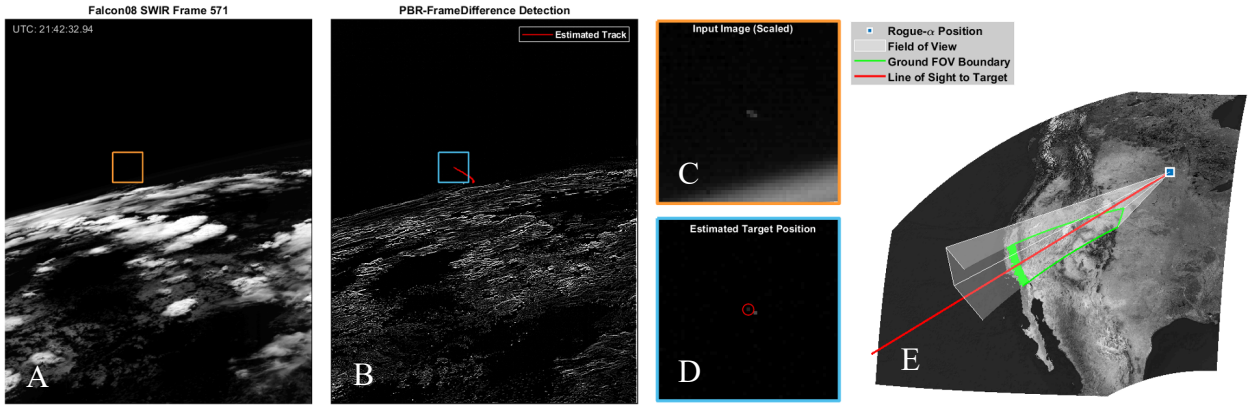

Figure 11. Aug 12, 2022, Falcon 9 Starlink Launch snapshot at SWIR frame 176. A) Unprocessed, B) Processed track C) Unprocessed and D) processed frame detail. E) Geometry of the observation.

Oct. 4, 2022, Atlas V ULA SES-20, 21 Launch

The final launch observed was a United Launch Alliance Atlas V rocket mission with a payload of two geosynchronous communication satellites. The rocket launched during daylight at 21:36:00 UTC and proceeded on a westward trajectory after initial ascent. The Atlas V uses a RD180 kerosene / liquid oxygen core stage and three GEM 63 solid strap-on boosters giving it an initial thrust of approximately 2 million lbs., somewhat larger than the Falcon 9 (approximately 1.7 million lbs. for the first stage). To avoid saturation of solar illuminated high cloud backgrounds, the SWIR camera integration was set to 2ms, the shortest of any of our rocket observation experiments. Rogue-α tracked the launch from 21:36:14.42 to 21:38:00.43 UTC. Track was lost at T0+120s, just after the solid boosters dropped off at T0+118s.[12] Figure 12 shows the SWIR imagery, *PBR-FrameDiff* processed data and track, and the geometry of the observation at 21:37:59.11 UTC, just before the track ends. The exhaust trail of the solid rockets is evident in the imagery. The CubeSat was over Georgia northwest

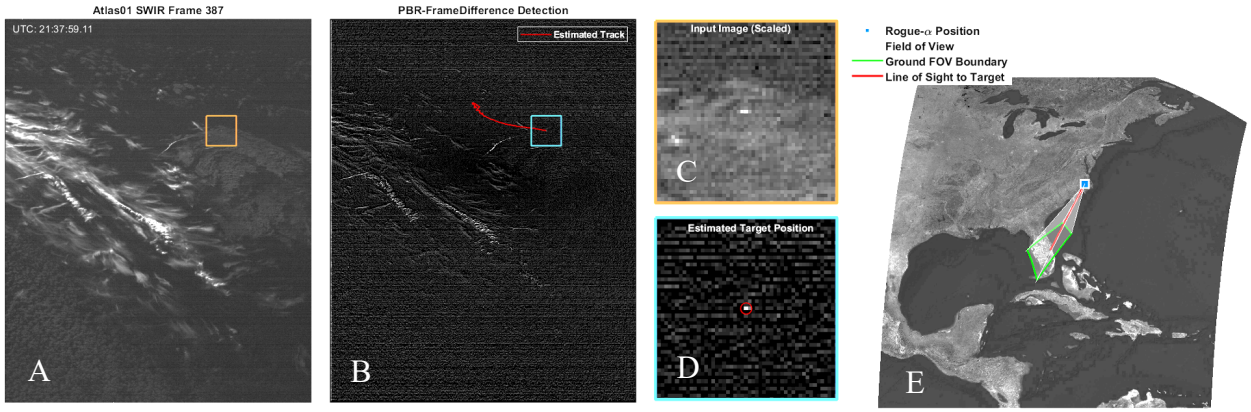

Figure 12. Oct 4, 2022, Atlas V ULA SES 20, 21 Mission snapshot at SWIR frame 387. A) Unprocessed, B) Processed Track, C) Unprocessed and D) Processed frame detail. E) Geometry of the observation.

of Cape Canaveral at start of track and orbited northeast to over North Carolina at end of track. The orbital geometry caused the initial track to change direction on the focal plane as the sensor orbited from west to east of the Cape during the first 50 seconds of observation.

A spacecraft pointing maneuver was conducted to try to keep the rocket in sight as it moved west. This executed properly, but at high altitude, the Atlas V core stage had already dimmed below our detection threshold at the 2ms integration time setting chosen. Our successful last rocket experiment struck a balance between obtaining unsaturated daytime backgrounds and detecting targets of varying brightness and range.

Novel CubeSat Observations of Aircraft

The Rogue-α,β sensors repeatedly observed large natural gas flares to study our sensor's performance and pointing accuracy. During a frame co-registration study of flare targets observed on September 3, 2021, moving features in the 1.4μm band SWIR video were noticed. Close study of two minutes of data revealed a number of these "moving" features to be due to uncorrected bad or "blinking" pixels put into apparent motion by the rotation of the focal plane over the fixed targeted position in the center of the flare region.

Several moving targets remained, however, with tracks inconsistent with focal plane motion. Through enhanced processing, these were determined to likely be aircraft flying straight line tracks on a northwest heading at typical civil airliner velocities. The signals are believed to be solar scattering and reflection from the large wingspan area of civil airliners, and appear as weak constant signals, rather than short specular flashes.

Detection of aircraft in flight by commercial imagery systems is not new,[13] but to our knowledge, this is the first time a remote sensing CubeSat has observed a moving aircraft in a way that a track could be formed. Aircraft have been tracked using RF signal reception by CubeSats built by commercial companies, including GOMSPACE, SPIRE and others.[14] Comparison of our results to these types of commercial RF data, or ground-based data, would be useful to confirm our observation.

Figure 13 shows a raw frame of the region, a processed frame with aircraft detections highlighted and an enhanced, contrast stretched image highlighting the targets. Sophisticated image-based frame stabilization, and robust temporal, spatial background suppression, were employed to filter and track the dim moving targets. The images shown in Figure 13 depict: A) bad-pixel corrected image frame 46 (the "north up" reference frame chosen for frame stabilization), B) the background-suppression processed frame 45 with circles around the moving aircraft targets, and C) contrast enhanced frame 45 with the aircraft targets circled.

Calculated velocities for the objects were found to be approximately 550-520mph at 33,000-36,000 feet respectively, which reinforced our hypothesis that these are large civil airliners. The location is also on known flight paths for commercial air traffic from the Persian Gulf. Pointing-based registration frame stabilization was also studied for these data, but false alarm and tracking results were better using image-stabilized frames.

Figure 14 shows: A) candidate tracks which are mostly residual focal plane artifacts, B) the surviving tracks after focal plane artifact motion was rejected, and C) the signal to noise ratio of these three tracks. 140 frames were selected for study from the 420 frame, 1hz frame rate collect. For data other than the central two minutes of data near nadir, the longer ranges and more extreme viewing angles made image-based frame alignment processing and dim target detection impractical. The SWIR imagery was taken at 10ms exposure, which was long for a typical daytime scene. The desert scene

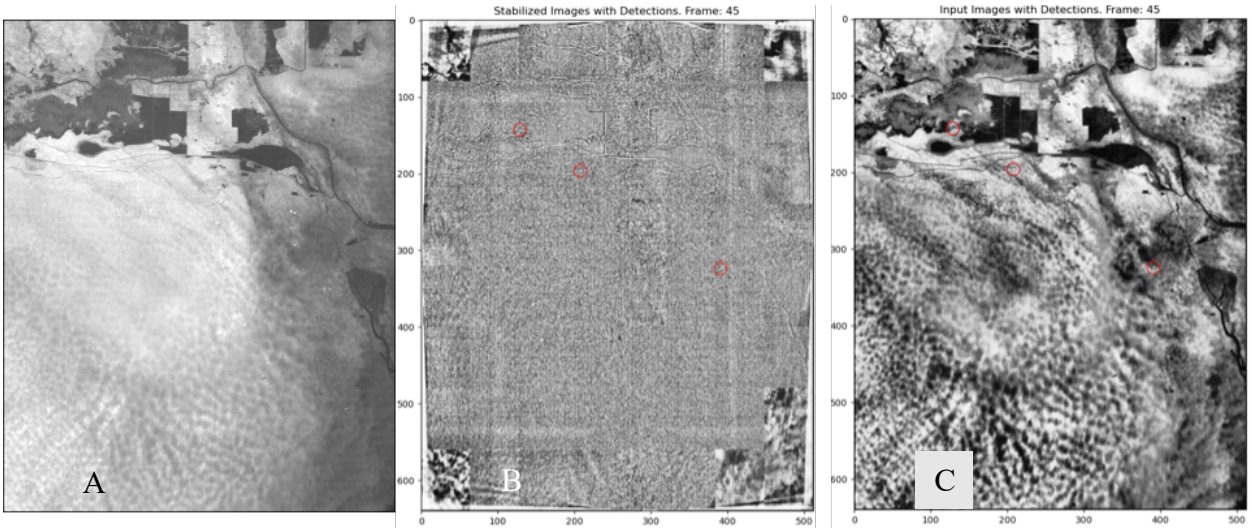

Figure 13. Detection of aircraft illustrated using a single data frame. A) Bad pixel corrected IR data. B) Background suppressed data with tracked signals (red circles). C) Stretched data showing the tracked signals (red circles). Image-based frame registration was used to facilitate tracking dim targets. The frames shown were from the north-oriented reference frame (north is up). Data were taken by Rogue-β taken of a gas flare region near Basra, Iraq on Sep. 3, 2021.

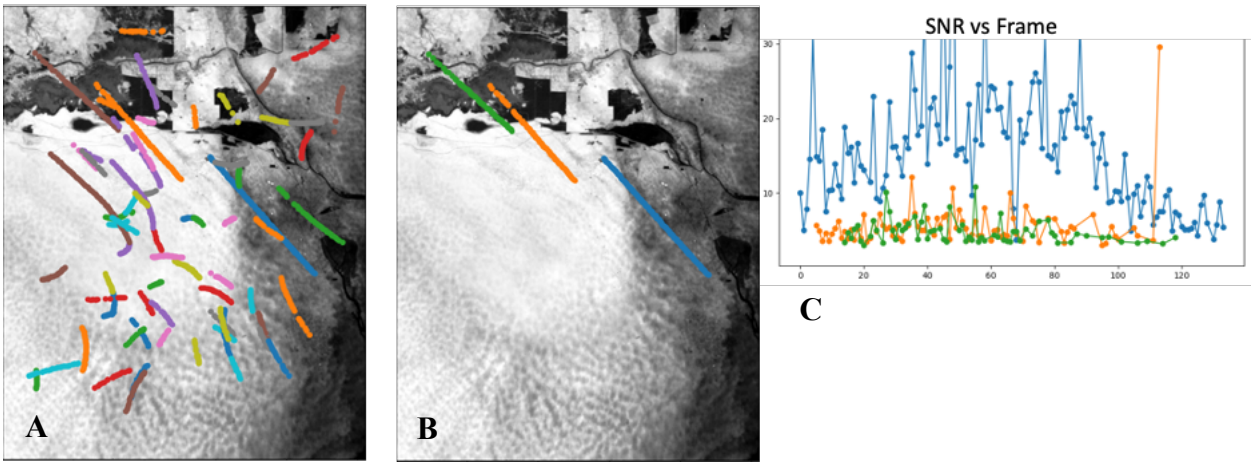

Figure 14. A) All tracks. B) Tracks following residual focal plane artifact rejection. C) Signal to noise for the three target tracks. The median S/N ratio was: 13.7 (blue track), 5 (orange track), and 4.5 (green track).

ended up somewhat underexposed due to the lack of any clouds, however the brightest flare source was saturated.

Additional Rogue-α,β experiments have been tasked over busy airports regions and additional aircraft tracked. Data taken in the United States are being studied to gather more examples for comparison with the robust flight tracking data available from ground-based air traffic control systems to follow up on this initial work.

Application of Pointing-based Registration to Rogue–α,β Wildfire Smoke and Fireline Observations

Our initial use of pointing-based registration techniques for cloud altitude determination was reported in an earlier paper.[3] In that work manual stereo correlation of two image frames spaced by 30-60 seconds was used to estimate cloud top heights for tropical cyclones and wildfire pyrocumulonimbus clouds and smoke plumes.[3] To advance beyond a manual approach we studied methods of automating this process. This was done by quantitative correlation of features between a reference frame and the paired PBR frame as a function of altitude. The PBR frame was used to create an array of frames varied by target altitude from sea level to 50,000ft. These were then correlated to the reference frame in localized pixel zones to find the best matches across a scene. Interesting results were obtained, creating 3D fire and

cloud scenes for several serious western USA wildfires in the Sierra Nevada including the Dixie and Caldor fires. An example from one of the Rogue-a,β Dixie fire observations is used to illustrate the technique below.

Figure 15 illustrates the two near-nadir frames chosen from a 5-minute observation of the Dixie fire for use in the PBR technique. The two selected observations were 30 seconds apart at 00:15:37.43 and 00:16:07.44 UTC on Aug. 6, 2021. Figure 16 shows the image correlation altitude map results. The volume plot is an image from an animated three-dimensional rendering of the Dixie fire smoke plume scene. The animated graphics, which vary the aspect angles, display the results somewhat better. Altitudes can be determined in regions with strong correlated features. Regions with weak image structure, and areas where the 10ms sensor exposure saturated cloud and smoke features, left gaps in the scene. Nonetheless, we were pleased with these initial results. For staring sensors, the technique could find use in determining cloud top heights, particularly smoke cloud heights, for which standard weather satellite atmospheric cloud altitude retrievals from thermal IR methods do not work well. Related 3-D cloud scene work has been proposed and recently performed by other sensors, including a visible sensor hosted by a CubeSat.[15,16] Our work, uniquely, used a wider field of view infrared waveband sensor, and was applied to wildfire pyrocumulonimbus clouds and smoke plumes.

An additional use of the PBR method we explored during our wildfire studies was creating frame stabilized videos of actively burning fire lines. By selecting 30-60 seconds near nadir from our 1hz frame rate SWIR measurements of wildfires, a short video of the targeted region could be created. These proved useful for revealing wildfire activity. All PBR frames are rotated into the reference frame coordinates at the altitude of the targeted region. As discussed above, animations can better show this, but Figure 17 shows three still frames zoomed in on the Dixie fire line from a 40-second portion of the Rogue-α Aug. 6, 2021, observation. Subtle intensity fluctuations are evident, especially along the hottest parts of the fire line. In an animation, intensity fluctuations and flickering are distinctly observed, and the motion of a convective smoke plume from the most intense burning region of the scene can be readily seen. Data of this sort are obtainable from loitering platforms such as helicopters, however, we haven't seen any infrared wildfire data from a low-Earth orbiting CubeSat processed into a motion video product before this work. Evidence of this type of flame intensity dynamics was seen in other Rogue-α,β wildfire observations, as well as in our flare observations, but the extreme fire behavior of the Dixie fire made the phenomenon particularly easy to observe in a PBR frame stabilized video.

Support for fighting wildland fires from satellites is a growing area of research and investment. The use of both government and commercial satellites is a topic of active study. Our work in recent years with both the CUMULOS CubeSat IR sensors and the Rogue-a,β VIS and SWIR sensors illustrates that useful fire monitoring observations can be performed with simple staring imaging sensors on small satellites.[2,3,5] Staring sensors allow for 3D processing and video capture that complement the wide-area mapping capabilities of scanning sensors such as VIIRS, MODIS, Landsat and Sentinel. Useful fire monitoring missions should be achievable with future staring infrared sensors, especially if the data are transmitted to emerging low-earth-orbiting communications constellations for real-time exploitation and use.

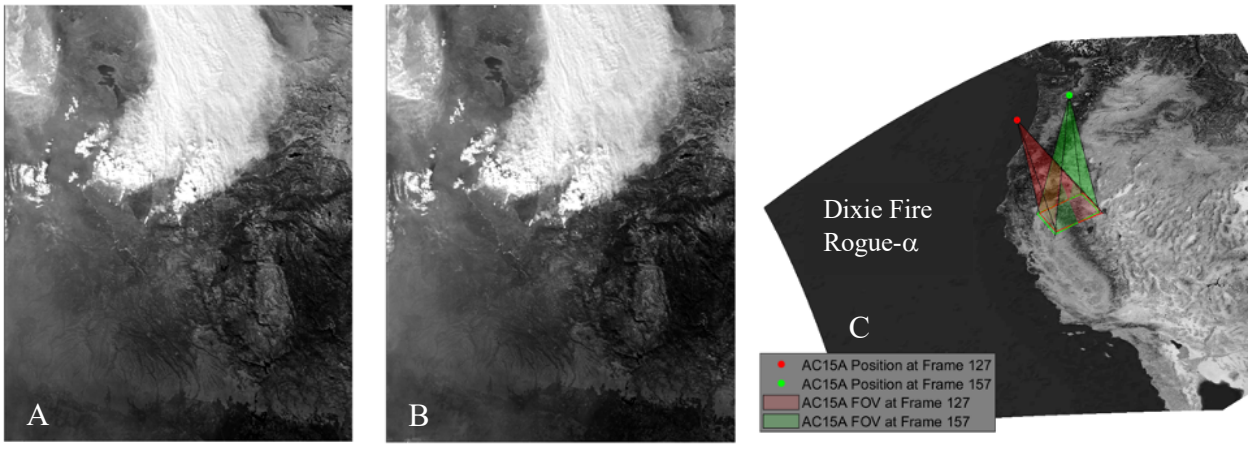

Figure 15. A) SWIR reference frame 127. B) PBR frame 157. C) Geometry of the two observations used with pointing-based registration for three-dimensional analysis of the Dixie fire on Aug. 6, 2021.

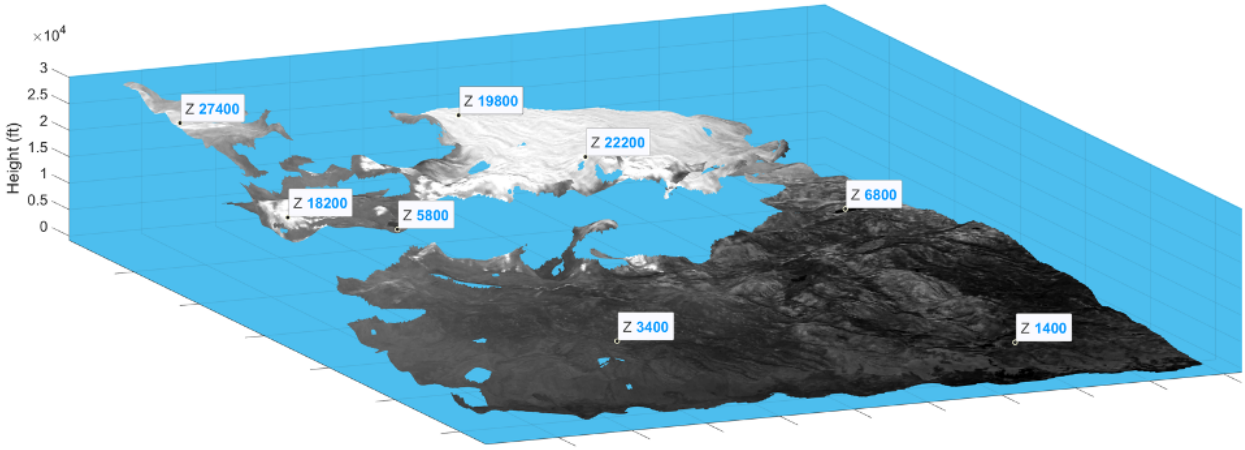

Figure 16. Three-dimensional analysis results of the Dixie fire smoke plume and surrounding Sierra Nevada terrain. The smoke plume lofted to approximately 20kft as determined by automated feature correlation using two frames from measured 30 seconds apart.

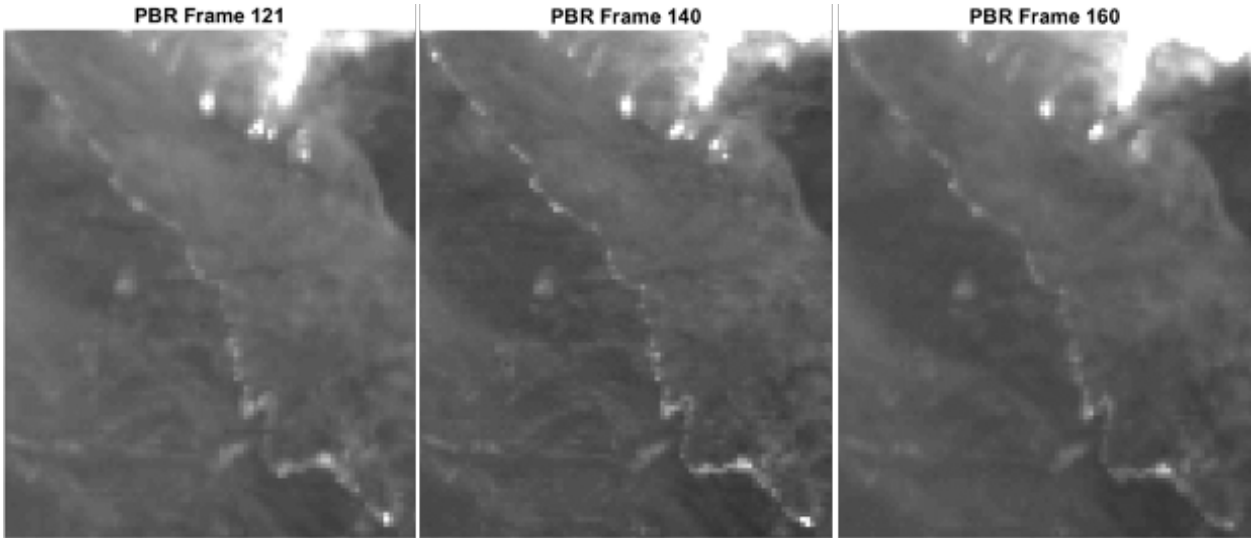

Figure 17. Three Rogue-α frames animating the SWIR fire line signal from the Aug. 6, 2021, Dixie fire observation. Flame front intensity fluctuations and smoke plume motion are evident, especially in the full PBR frame animation. This SWIR imagery was taken through smoke which obscured the simultaneous visible context camera view of the scene.[3]

CONCLUSIONS

This paper completes a series of Small Satellite Conference papers documenting the engineering and flight operations of the Rogue-α,β CubeSats, agile 3-axis stabilized spacecraft, equipped with infrared and visible sensors as well as a compact laser communications payload. The first three papers and associated briefings covered the engineering build, initial operational successes, and environmental remote sensing results for which staring motion video was an enabling capability. This paper summarized all the Rogue-α,β CubeSat observations of rocket launches, eight in total, six described here for the first time, and outlined some of the processing approaches used to analyze them. Simple frame differencing, spatial and temporal filtering, anomaly detection, and pointing-based registration of frames were among the techniques utilized to help track space launches with our novel 1.4μm band infrared fast framing sensor. Image-based registration combined with spatial and temporal filtering were able to detect unexpected probable aircraft motion in several experiments. New data exploitation techniques were also applied to Rogue-α,β observations of severe wildfires.

Pointing-based registration (PBR) was used on wildfire data in two different ways. First, PBR was used to determine cloud heights via stereo correlation of two selected frames from an orbital collect. This technique was automated and applied to determine the height of general cloud scenes, severe storms and, as shown in this paper, wildfire pyrocumulonimbus clouds and smoke plumes. Second, PBR was used to create active fire line videos via registering multi-frame observations near-nadir to reveal dynamic fire activity. Both techniques should find application in operations of future staring IR sensors for fire monitoring missions.

MISSION SUMMARY

Each period of the Rogue-α,β mission held interesting lessons for those involved in the project. The engineering lessons were summarized our first paper, and we benefited from our CubeSat program science and engineering teams streamlined, but sufficient requirements definition and program review processes.[1]

Careful preparation of both an on-orbit spacecraft test plan and flight experiment plan allowed the first year of operations, described in our second paper, to fulfill the program's requirements for success.[2] Calibration of the visible and infrared sensors using bright standard stars was demonstrated. Laser pointing was aligned on orbit between spacecraft to speed up laser communications operations. A novel 1.4µm SWIR band was characterized for Earth observation for the first time. The ability of the SWIR sensor to observe gas flares, terrestrial and cloud backgrounds, rockets, severe weather, wildfires other IR targets was accomplished. Initial stereo observations were also carried out along with other spacecraft ConOps. A data pipeline was finalized which processed the Rogue-α,β sensor data and associated metadata into convenient standard formats for exploitation.[2]

We were able to continue operations beyond one year, and an extended operations plan was pursued. The next year on-orbit focused on adding to our observations of space launches, additional IR targets and backgrounds. Sensor settings were honed to better reveal wildfire activity in the 1.4µm SWIR band as well as to obtain multiple, well-exposed multi-minute orbital data sets on storms and Earth backgrounds. Unique staring sensor data were acquired for large wildfires, hurricanes, and tornadic thunderstorms. Nighttime sensor data were collected, including from our narrow-field-of-view star sensor. We described highlights from these environmental observations in our third paper.[3] Additional rocket observations gathered during this second year of operations were not fully analyzed and published until this paper.

Our focus shifted to data exploitation in our final year of spacecraft operations. We continued collecting data with an emphasis on rocket observations, especially daytime observations, for which opportunities had previously been elusive. We eventually succeeded in observing several launches under daylit conditions. Our entire rocket observation experiment series is described in this paper, showing our successes in tracking Falcon 9, Soyuz, Long March, and Atlas V space launches from different types of orbital geometries against Earth and space backgrounds. Data from both the rocket experiments, and the environmental observations, were used to study a variety of detection algorithms, and used to develop pointing-based and image-based registration approaches for deeper analysis.

The Rogue-α,β CubeSat experiments illustrated what can be accomplished with small, agile-pointing, spacecraft platforms equipped with staring visible and IR sensor payloads. Future proliferation of low-Earth orbit wide-field-of view sensors will open new possibilities for remote sensing. The data collected by Rogue-a,β experiments should be of interest to other small satellite researchers, and we hope the experiments and satellite use modes demonstrated will be useful as guides to future work by our academic, industry, and government colleagues.

REFERENCES

1. Navarro, M., Gussy, J. Pack, D., Rowen, D. and Salvaggio, D 2020. "Building Satellites in 18 Months: Lessons Learned from the Rogue Alpha/Beta CubeSats," *Proceedings of the AIAA/USU Conference on Small Satellites*, Year in Review, SSC20-II-07, https://digitalcommons.usu.edu/smallsat/2020/all2020/116/

2. Pack, D., Hardy, B., Santiago, J., Pietrowski, D., Mauerhan, J. et al. 2021, "Flight Operations of Two Rapidly Assembled CubeSats with Commercial Infrared Cameras: The Rogue-Alpha,Beta Program", Proceedings of the AIAA/USU Conference on Small Satellites, Year in Review, SSC21-III-03, https://digitalcommons.usu.edu/smallsat/2021/all2021/149/

3. Pack, D., Thiyanaratnam, P., Freeze, T., Hardy, B., Santiago, J., Pietrowski, D., Mauerhan, J., Johnson, P., Zittel, P., Purcell, C., "Remote Sensing experiments using the Rogue-alpha,beta CubeSats as a constellation: high frame rate environmental observations from agile, taskable, infrared and visible sensors in low Earth orbit**",** Proceedings of the AIAA/USU Conference on Small Satellites, (SMALLSAT) 2022. http://digitalcommons.usu.edu/smallsat/2022/all2022/111

4. Pack, D.W., D.R. Ardila, E. Herman, D.W. Rowen, D.W., R.P. Welle, S.J. Wiktorowicz, and B.W., Hattersley, 2017. "Two Aerospace Corporation CubeSat Remote Sensing Imagers: CUMULOS and R3", *Proceedings of the AIAA/USU Conference on Small Satellites*, Next on the Pad, SSC17-III-05, https://digitalcommons.usu.edu/smallsat/2017/all2017/82/.

5. Pack, D.W., C.M. Coffman, J.R. Santiago, 2019. "A Year in Space for the CubeSat Multispectral Observing System: CUMULOS", *Proceedings of the AIAA/USU Conference on Small Satellites,* Year in Review SSC19-XI-01, https://digitalcommons.usu.edu/smallsat/2019/all2019/148/.

6. Rose, T., D.W. Rowen, S. LaLumondiere, N.I. Werner, R. Linares, A. Faler, J. Wicker, C.M. Coffman, G.A. Maul, D.H. Chien, A. Utter, R.P. Welle, S.W. Janson, 2018. "Optical Communications Downlink from a 1.5U CubeSat: OCSD Program", *Proceedings of the AIAA/USU Conference on Small Satellites*, Assuring the Space Ecosystem, SSC18-XI-10,

7. Mauerhan, J., Pack, D., Santiago, J., Hardy, B., Zittel, P. 2021. "Radiometric Calibration of AeroCube 15 (Rogue-Alpha,Beta), *Conference on Characterization and Radiometric Calibration for Remote Sensing (CALCON).* https://digitalcommons.usu.edu/calcon/CALCON2021/all2021content/8/

8. See video: Arianespace/Starsem Soyuz 2.1b - One Web 11 Cosmodrome Vostochny October 14, 2021. https://www.youtube.com/watch?v=VjRaOHvNeZg

9. See mission summary and launch trajectory at: https://www.russianspaceweb.com/oneweb11.html

10. See SpaceX video: COSMO-SkyMed Second Generation FM2 Mission. https://www.youtube.com/watch?v=zBxHrNIzp9w

11. See SpaceX Starlink video: https://www.youtube.com/watch?v=SU5FbiCbjic

12. Source: https://www.ulalaunch.com/missions/archived-launched/atlas-v-ses-20-ses-21

13. See for instance, Krauß, T.: Exploiting Satellite Focal Plane Geometry for Automatic Extraction of Traffic Flow from Single Optical Satellite Imagery, Int. Arch. Photogramm. Remote Sens. Spatial Inf. Sci., XL-1, 179–187, https://doi.org/10.5194/isprsarchives-XL-1-179-2014, 2014

14. Leon, L., Koch, P., Walker, R. 2018. "GOMX-4 – The Twin European Mission for IOD Purposes", *Proceedings of the AIAA/USU Conference on Small Satellites, Science/Mission Payloads II*, SSC18-VII-07 https://digitalcommons.usu.edu/smallsat/2018/all2018/296/

15. Castro, E.; Ishida, T.; Takahashi, Y.; Kubota, H.; Perez, G.J.; Marciano, J.S. "Determination of cloud-top Height through three-dimensional cloud Reconstruction using DIWATA-1 Data", Sci. Rep. 2020, 10, 1–13.

16. Tzabari, M, Holodovsky, V, Shubi, O, Eytan, E Altaratz, O, Koren, I, Aumann, A, Schilling, K, Schechner, Y, "CloudCT 3D volumetric tomography: Considerations for imager preference, comparing visible light, short-wave infrared, and polarized imagers," in Polarization Science and Remote Sensing X, vol. 11833. International Society for Optics and Photonics, 2021, p.1183304.